ACS OMEGA

http://pubs.acs.org/journal/acsodf

Article

Defect-Induced Inhomogeneous Phase Transition in 2D Perovskite Single Crystals at Low Temperatures

Zixi Yin, Jing Leng,* Chunyi Zhao, Junxue Liu, Boning Wu, and Shengye Jin*

Cite This: *ACS Omega* 2021, 6, 35427−35432

Read Online

ACCESS | Metrics & More | Article Recommendations | Supporting Information

ABSTRACT: The temperature-induced phase transition in two-dimensional (2D) layered perovskites was recently found to be incomplete even if the temperature dropped to tens of kelvin. However, its intrinsic cause still remains unclear, and the information on the phase transition in individual single crystals (SCs) is also limited. Herein, we study the phase transition process in individual $(n\text{-}C_4H_9NH_3)_2PbI_4$ SCs using a home-built photoluminescence (PL)-scanned image microscope. At 83 K, the phase transition is indeed incomplete, leading to the coexistence and inhomogeneous distributions of room-temperature and low-temperature phases. We map the distribution of phase transition degree on individual SCs at 83 K, which exhibits a strong positive (negative) correlation with the distribution of local defects (PL lifetimes) at 293 K, indicating that the phase transition is enhanced by initial defects. Our findings might provide new insight into the phase transition of $(n\text{-}C_4H_9NH_3)_2PbI_4$ crystals, which is of potential value for applications based on 2D layered perovskites.

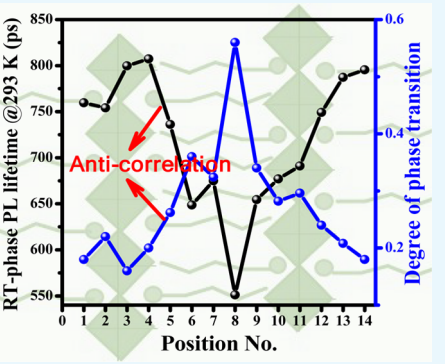

INTRODUCTION

Two-dimensional (2D) layered Ruddlesden−Popper lead-halide perovskites are a class of semiconductor materials with a general formula of $(RNH_3)_2(A)_{n-1}M_nX_{3n+1}$, where RNH_3^+ is an ammonium cation with a long hydrophobic side chain, A^+ is a small cation like $CH_3NH_3^+$, M^{2+} is a metal cation, and X^- is a halide anion. They are naturally formed multiple-quantum wells, which are composed of n layers of lead halide octahedrons segregated by insulating ligands.[1−3] Compared to their three-dimensional (3D) analogues, layered 2D perovskites exhibit better moisture resistance, higher photostability, larger exciton binding energies, and tunable bandgaps due to the presence of the hydrophobic and length-adjustable organic ligands.[1−10] These properties make 2D perovskites display great potential in the fabrication of solar cells, light-emitting diodes, and other optoelectronic devices.[11−16]

Another attractive feature of 2D perovskites is their tunable optical properties with the change of environmental conditions.[17−21] Notable success has been achieved in regulating the optoelectronic properties through the phase transition process by adjusting the temperature.[21−24] Previous reports have shown that $(RNH_3)_2PbX_4$, as a series of single-layer (n = 1) perovskites, exhibits a reversible phase transition when the temperature decreases.[25−27] Whittaker-Brooks and co-workers observed an abrupt phase transition at ∼250 K in an $(n\text{-}C_4H_9NH_3)_2PbI_4$ thin film, and its band energy increased from 2.4 eV at room temperature (RT) to 2.53 eV at low temperature (LT) at the same time.[28] Nag and co-workers compared the phase transition in single crystals (SCs) and exfoliated few-layer lattices of the same compound and found that their phase transitions display different hysteresis behaviors during heating/cooling cycles. Such a phase transition is found to be incomplete even though the temperature drops to tens of kelvin, leading to a biphase structure revealed by dual-color emission at low temperatures.[29]

Similar incomplete phase transitions were also observed in 3D hybrid perovskites and were usually considered to be correlated with structural defects (e.g., vacancies or dangling bonds). It was proposed that the existence of defects can change the lattice strain and thereby improve the phase transition completeness by facilitating the tilt and distortion of the lattice during the phase transition process.[30,31] However, the experimental evidence for this mechanism is still lacking. Herein, we study the temperature-induced phase transition in $(n\text{-}C_4H_9NH_3)_2PbI_4$ 2D perovskite SCs. By using a home-built photoluminescence (PL)-scanned imaging microscope, we map the PL emission on individual 2D perovskite SCs (with a few μm in lateral dimension) from both LT and RT phases at different temperatures. We find that the 2D perovskite SCs exhibit a spatially inhomogeneous phase transition starting from ∼263 to 83 K, and the completion degree of the local phase transition shows a strong negative correlation with the spatial distribution of local PL lifetimes on the SCs at room

Received: September 1, 2021
Accepted: November 24, 2021
Published: December 14, 2021

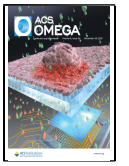

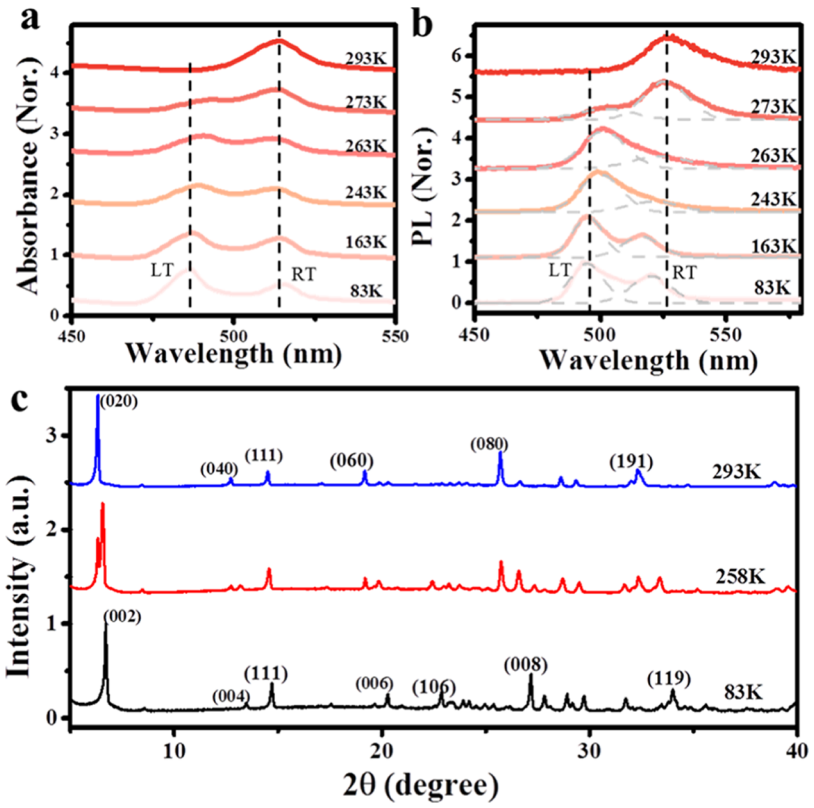

Figure 1. Temperature-dependent absorption (a) and PL (b) spectra of $(n\text{-}C_4H_9NH_3)_2PbI_4$ crystals collected at various temperatures from 83 to 293 K. The excitation wavelength is 405 nm for PL measurements. The gray dashed lines in (b) are Gaussian fits of the spectra, separating the contributions from LT and RT phases. (c) Temperature-dependent X-ray diffraction (XRD) patterns of $(n\text{-}C_4H_9NH_3)_2PbI_4$ SCs at indicated temperatures.

temperature, whose variation is likely caused by the change of local structural defects. We believe that this result experimentally establishes the correlation between the phase transition and structural defects in perovskite materials, thus shedding light on the control of the phase transition of 2D layered perovskites.

RESULTS AND DISCUSSION

The $(n\text{-}C_4H_9NH_3)_2PbI_4$ SCs were prepared via a method reported in previous literature,[32] and the experimental details are provided in the Supporting Information (SI). Transmission electron microscopy (TEM) and selected area electron diffraction (SAED) analyses were performed to evaluate the quality of $(n\text{-}C_4H_9NH_3)_2PbI_4$ SCs. As shown in Figure S1a, the as-synthesized $(n\text{-}C_4H_9NH_3)_2PbI_4$ SC shows a neatly arranged point-like diffraction pattern, indicating that the $(n\text{-}C_4H_9NH_3)_2PbI_4$ SC is of high quality. For UV−Vis absorption, PL spectroscopy and imaging measurements, mechanically exfoliated 2D SCs were prepared and transferred on glass coverslips. The UV−Vis absorption spectra and PL emission spectra of an ensemble of $(n\text{-}C_4H_9NH_3)_2PbI_4$ SCs (see Figure S1b for an optical image) collected at various temperatures ranging from 83 to 293 K are shown in Figure 1a and 1b, respectively. At room temperature (RT, 293 K), the 2D crystals show a single absorption peak centered at 514 nm, which is the first-exciton absorption of $(n\text{-}C_4H_9NH_3)_2PbI_4$ 2D perovskite quantum wells. As the temperature decreases, a high-energy absorption peak near 490 nm gradually appears and becomes more prominent (narrower and sharper) at low temperatures. This change in the absorption spectra is indicative of the temperature-induced phase transition of $(n\text{-}C_4H_9NH_3)_2PbI_4$ 2D perovskites from the RT phase (~514 nm) to the LT phase (~490 nm),[28] which starts around 263 K. An interesting phenomenon in the phase transition process is that the RT-phase absorption (~514 nm) persists over the temperature tuning range, suggesting that the phase transition in $(n\text{-}C_4H_9NH_3)_2PbI_4$ 2D perovskites is incomplete even at 83 K. Exactly consistent with the absorption spectra, the PL spectra of the 2D perovskites exhibit a similar temperature-induced spectral evolution (Figure 1b), and the dual emission bands of 494 nm from the LT phase and 520 nm from the RT phase at low temperatures can be well separated by Gaussian fits, again suggesting the incomplete RT-to-LT phase transition at low temperatures. These observations in absorption and PL spectra agree well with those in the literature,[28,29] confirming that the incomplete temperature-induced phase transition is a common phenomenon in hybrid 2D perovskites with $n = 1$.

Temperature-dependent powder XRD characterization was also performed on $(n\text{-}C_4H_9NH_3)_2PbI_4$ crystals. As shown in the XRD patterns (Figures 1c and S2), the diffraction peaks from the LT phase ((002), (004), (006), (008)) become weaker and disappear eventually when the temperature increases from 83 to 293 K, and meanwhile the diffraction peaks from the RT phase ((020), (040), (060), (080)) gradually appear and become stronger. These results, together with the above absorption and PL spectra, indicate that the structural phase transition occurs near 263 K, which agrees with the previous reports by Nag et al. and Billing et al.[27,29] Moreover, the transition temperature is also similar to that from the differential scanning calorimetry (DSC) data reported

https://doi.org/10.1021/acsomega.1c04800
ACS Omega 2021, 6, 35427−35432

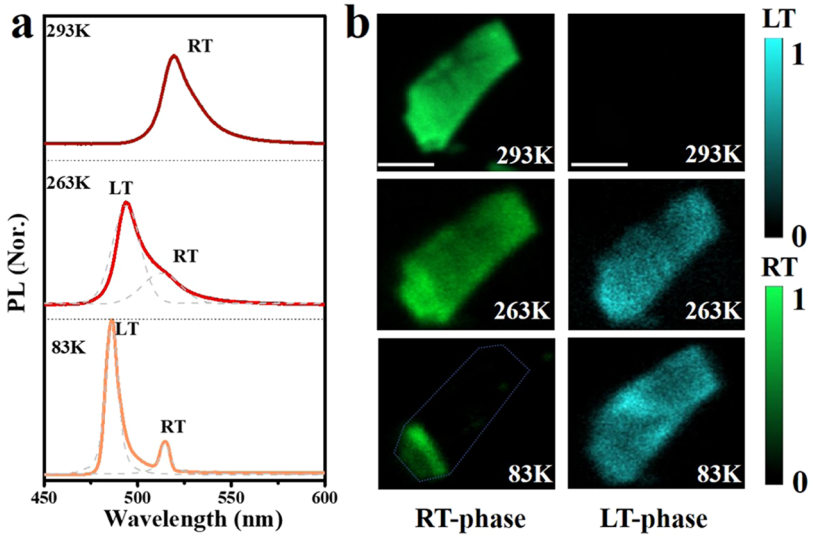

Figure 2. (a) Temperature-dependent PL spectra of an exfoliated $(n\text{-}C_4H_9NH_3)_2PbI_4$ crystal under 405 nm excitation. The gray dashed lines are the Gaussian fits of the spectra, showing contributions from RT and LT phases. (b) PL intensity images of the same exfoliated crystal as in panel (a) collected in the emission channels of 470−490 nm for the LT phase (blue) and 515−535 nm for the RT phase (green) at indicated temperatures under 405 nm excitation. The scale bars are 10 μm.

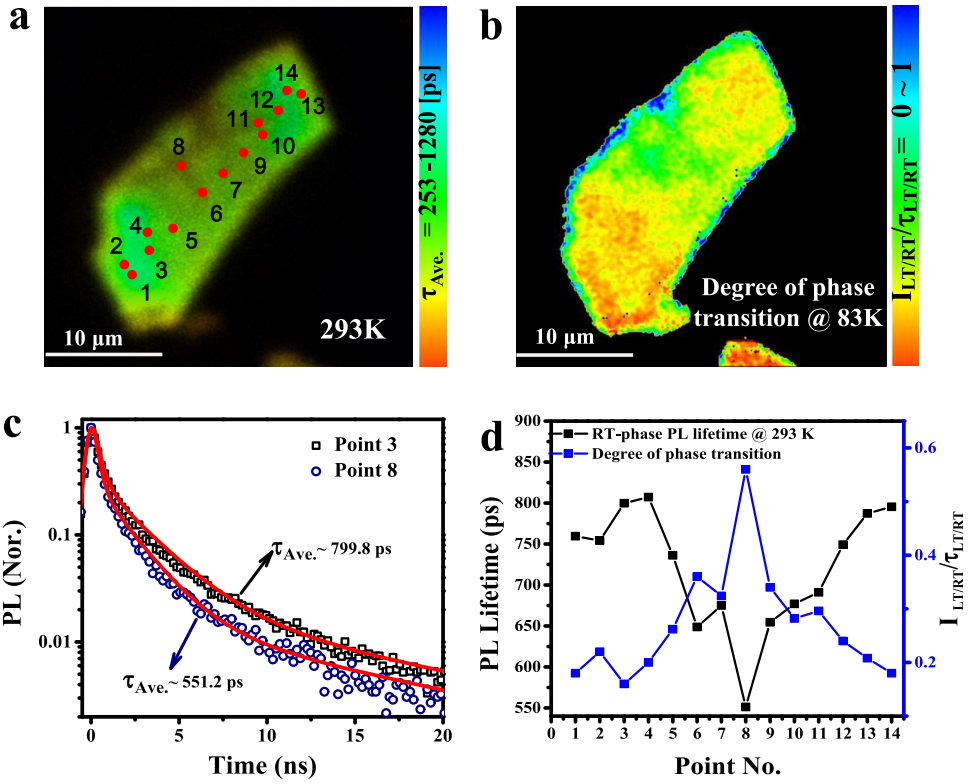

Figure 3. (a) RT-phase PL lifetime map measured on an individual $(n\text{-}C_4H_9NH_3)_2PbI_4$ crystal at 293 K. (b) Map of relative completion degree of phase transition at 83 K (normalized at maximum) calculated according to eq S4 in the SI, showing a clear inverse correlation relative to the RT-phase PL lifetime image in panel (a). (c) PL kinetics of the RT-phase measured at 293 K at typical positions as shown in (a); red lines are their fitting curves. (d) Comparison of the RT-phase PL lifetimes and relative degrees of phase transition at various positions (denoted by red points) as shown in panel (a).

by Nag et al.,[29] further confirming that the change in PL spectra at lower temperatures does result from the change in the structure of the SC. One difference is that we do not observe the RT-phase diffraction peaks in XRD patterns while the temperature drops below 243 K (Figure S2), which might be attributed to the limited detection depth and sensitivity of XRD measurements.

The carrier dynamics in $(n\text{-}C_4H_9NH_3)_2PbI_4$ SCs at different temperatures were also examined by performing transient absorption (TA) measurements (see the SI for a detailed description of TA measurements). Briefly, a pump pulse at 400

https://doi.org/10.1021/acsomega.1c04800
ACS Omega 2021, 6, 35427−35432

nm is used to excite the sample, and the induced absorption changes (ΔA) are recorded as a function of both wavelength and time. The excitation intensity is 1.4 $\mu J/cm^2$, which is within the linear response range (Figure S3). Figure S4 compares the TA spectra of $(n\text{-}C_4H_9NH_3)_2PbI_4$ SCs measured at room temperature and low temperatures. Consistent with their steady-state absorption spectrum, their TA spectrum at room temperature shows a single bleach peak at 516 nm due to the band-edge exciton filling, which then splits into discrete LT-phase and RT-phase bleach peaks with the decrease of temperature (Figure S4d). These two bleach peaks exhibit independent TA kinetics at low temperatures (see Figure S5), suggesting that there is no charge or energy transfer between the two phases even when they are coexisting. Both LT and RT phases exhibit faster TA kinetics as the temperature decreases, likely because of the larger relative proportion of the excitons at low temperatures in 2D perovskites.[33]

To elucidate the factors that affect the phase transition, we examined the PL spectra and intensity images from an individual exfoliated $(n\text{-}C_4H_9NH_3)_2PbI_4$ SC (with the lateral dimension of tens of μm; see Figure S6a for its optical image) at different temperatures using a home-built PL-scanned imaging microscope. The PL spectra from an individual exfoliated SC also exhibit two emission peaks from RT and LT phases as the temperature decreases (Figures 2a and S6b), and similar PL spectra are also observed in many other $(n\text{-}C_4H_9NH_3)_2PbI_4$ SCs (Figure S7). However, the PL intensity ratio between RT and LT phases varies significantly between different SCs, suggesting that the completion degree of the phase transition varies in different SCs. Besides the two PL peaks from RT and LT phases, a weak and broad emission from 550 to 704 nm is also observed in some SCs at 83 K (Figure S8a,c). This low-energy emission is likely related to the emission of self-trapped excitons (STEs) and/or defect states,[22] which usually exhibit much longer PL lifetime as shown in Figure S8b and S8d.[34−36]

Figure 2b shows a set of PL intensity images from a typical SC (the same crystal as shown in Figure 2a) at different temperatures (see Figure S9 for images at other temperatures). The images for LT and RT phases are distinguished by collecting the PL at different wavelength channels of 470−490 nm for the LT phase and 515−535 nm for the RT phase. The RT-phase PL is relatively homogeneously distributed at room temperature but gradually becomes more and more inhomogeneous when the temperature drops below 263 K, and the distribution of the RT phase is roughly inversely related to that of the LT phase. In other words, where the RT-phase PL is stronger, the LT-phase PL is weaker. This indicates that the inhomogeneous PL distributions of RT and LT phases at low temperatures result from the inhomogeneous phase transition in the SC. Stronger RT-phase PL represents less LT-phase transformation and vice versa. Similar inhomogeneous phase transition and inverse RT/LT-phase distributions are also observed in other $(n\text{-}C_4H_9NH_3)_2PbI_4$ SCs (see Figure S10).

Some recent reports have shown that local structural defects can trigger the phase transition in 3D perovskites.[30,31] Therefore, we speculate that the inhomogeneous phase transition in $(n\text{-}C_4H_9NH_3)_2PbI_4$ SCs at low temperatures is also related to their inhomogeneous defect distribution. Figure 3a shows the PL lifetime map at 293 K measured on the same $(n\text{-}C_4H_9NH_3)_2PbI_4$ crystal as in Figure 2. This image exhibits an inhomogeneous lifetime distribution, with the average lifetime value ranging from 400 to 830 ps. In a semiconductor crystal, the PL lifetime is determined by radiative and nonradiative decay constants; the latter is usually affected by the density of defects (e.g., structural defects), which can reduce the lifetime by the Shockley−Read−Hall (SRH) recombination and/or charge carrier trapping.[37−40] As the radiative decay constant is an intrinsic property of the semiconductor, the local variation of PL lifetime can reflect the variation of local defect density. Therefore, we believe that the local change of PL lifetime shown in Figure 3a reflects an inhomogeneous structural defect distribution likely formed during sample preparation. That is, the shorter the lifetime, the higher the defect density. Here, we define the degree of phase transition at 83 K as the ratio of $I_{LT/RT}/\tau_{LT/RT}$ (see the SI for detailed deduction), where $I_{LT/RT}$ ($\tau_{LT/RT}$) represents the ratio between the intensity (lifetime) of LT-phase PL at 83 K and the intensity (lifetime) of RT-phase PL at 293 K. The distribution of the calculated degree of phase transition from the same crystal as in Figure 3a is shown in Figure 3b. To correlate their dependence, several points are selected and their PL kinetics at 293 K are fitted by a double exponential function. Figure 3c shows the PL kinetics and fitting curves of two typical points, while the PL lifetimes of selected 14 points at 293 K and the degrees of transition to the LT phase at 83 K are directly compared in Figure 3d. The distribution of the degree of phase transition at 83 K is almost opposite to the PL lifetime distribution at 293 K, implying that a local site with more defects likely shows a more complete transition to the LT phase at 83 K. Therefore, we conclude that the defects in $(n\text{-}C_4H_9NH_3)_2PbI_4$ SCs can enhance the degree of phase transition to the LT phase at low temperatures, and the inhomogeneous phase transition is attributable to the initial uneven distribution of local defects when the sample is prepared. The defect-enhanced phase transition may be attributed to the stronger lattice distortion induced by local structural defects (e.g., I vacancies and/or I vacancy-related defects).[31] In addition, we still measured the PL spectra from the same $(n\text{-}C_4H_9NH_3)_2PbI_4$ SC at 83 K at a slower cooling rate and further examined the distribution of the degree of phase transition completion in this case (Figure S11), which is also inhomogeneous and almost opposite to the PL lifetime distribution at 293 K. More importantly, the phase transition process at a slower cooling rate was found to exhibit a slightly higher degree of phase transition and a lower inhomogeneity of phase distribution, which might be attributed to the fact that the crystal lattice can be more fully twisted and distorted during the slow cooling process.

More $(n\text{-}C_4H_9NH_3)_2PbI_4$ SCs were inspected using the same method, as shown in Figures S12−S14. In all of the samples we measured, the degrees of phase transition to the LT phase at 83 K are distributed roughly inversely to the RT-phase PL lifetimes at 293 K. These results suggest the universality of the inhomogeneous and incomplete phase transition in $(n\text{-}C_4H_9NH_3)_2PbI_4$ SCs at low temperatures. On the basis of these findings, we believe that the different extents of temperature-induced phase transition between various SCs are also due to their different distributions of local defects during sample preparation, as shown in Figures S6 and S7. Interestingly, similar defect-induced/triggered phase transition behaviors have also been observed in $MAPbI_3$ single crystals by Dobrovolsky et al.[30] and $CsPbCl_3$ nanocrystals by Sun et al.[31] This might suggest the universality of local structural defects in promoting the phase transition of lead-halide perovskites at low temperatures, which is likely related to the analogous types

https://doi.org/10.1021/acsomega.1c04800
ACS Omega 2021, 6, 35427−35432

of defects such as the distortion of the inorganic layer structure and halogen vacancies caused by the same PbX_6 octahedral structure.[30,31]

CONCLUSIONS

In summary, we systematically investigated the phase transition from the RT phase to the LT phase at low temperatures in individual $(n\text{-}C_4H_9NH_3)_2PbI_4$ SCs using a home-built photoluminescence (PL)-scanned imaging microscope coupled with a temperature control system. Our results show that, even if the temperature drops to 83 K, the phase transition process is still incomplete, leading to the coexistence of two distinctive phases in individual SCs. By mapping the spatial distribution of the inhomogeneous phase transition in an individual $(n\text{-}C_4H_9NH_3)_2PbI_4$ SC, we confirm that the degree of phase transition at low temperatures is positively correlated with the initial distribution of local defects during sample preparation, which is thus inhomogeneous. The local defects promote the phase transition probably by distorting local lattice structures. Our finding provides useful information on the phase transition of 2D $(n\text{-}C_4H_9NH_3)_2PbI_4$ SCs and might have potential value for applications based on 2D layered perovskites.

ASSOCIATED CONTENT

Supporting Information

The Supporting Information is available free of charge at https://pubs.acs.org/doi/10.1021/acsomega.1c04800.

Sample preparations; photoluminescence-scanned imaging microscope and TA experiment setup; structure characterization, and definition of the degree of phase transition (Figures S1−S14) (PDF)

AUTHOR INFORMATION

Corresponding Authors

Jing Leng − *State Key Laboratory of Molecular Reaction Dynamics and Dynamics Research Center for Energy and Environmental Materials, Dalian Institute of Chemical Physics, Chinese Academy of Sciences, Dalian 116023, China;* orcid.org/0000-0002-8454-4835; Email: ljjx@dicp.ac.cn

Shengye Jin − *State Key Laboratory of Molecular Reaction Dynamics and Dynamics Research Center for Energy and Environmental Materials, Dalian Institute of Chemical Physics, Chinese Academy of Sciences, Dalian 116023, China;* orcid.org/0000-0003-2001-2212; Email: sjin@dicp.ac.cn

Authors

Zixi Yin − *State Key Laboratory of Molecular Reaction Dynamics and Dynamics Research Center for Energy and Environmental Materials, Dalian Institute of Chemical Physics, Chinese Academy of Sciences, Dalian 116023, China; University of Chinese Academy of Sciences, Beijing 100049, China*

Chunyi Zhao − *State Key Laboratory of Molecular Reaction Dynamics and Dynamics Research Center for Energy and Environmental Materials, Dalian Institute of Chemical Physics, Chinese Academy of Sciences, Dalian 116023, China*

Junxue Liu − *State Key Laboratory of Molecular Reaction Dynamics and Dynamics Research Center for Energy and Environmental Materials, Dalian Institute of Chemical Physics, Chinese Academy of Sciences, Dalian 116023, China;* orcid.org/0000-0001-8349-1017

Boning Wu − *State Key Laboratory of Molecular Reaction Dynamics and Dynamics Research Center for Energy and Environmental Materials, Dalian Institute of Chemical Physics, Chinese Academy of Sciences, Dalian 116023, China;* orcid.org/0000-0003-2280-3448

Complete contact information is available at: https://pubs.acs.org/10.1021/acsomega.1c04800

Notes

The authors declare no competing financial interest.

ACKNOWLEDGMENTS

S.J. acknowledges the financial support from the MOST (2018YFA0208704, 2016YFA0200602), the National Natural Science Foundation of China (No. 21725305), and the Strategic Priority Research Program of CAS (No. XDB17000000). J. Leng acknowledges the financial support from the National Natural Science Foundation of China (No. 21773237).

REFERENCES

(1) Zhang, Q.; Chu, L.; Zhou, F.; Ji, W.; Eda, G. Excitonic Properties of Chemically Synthesized 2D Organic-Inorganic Hybrid Perovskite Nanosheets. *Adv. Mater.* **2018**, *30*, No. 1704055.

(2) Tsai, H.; Nie, W.; Blancon, J. C.; Stoumpos, C. C.; Asadpour, R.; Harutyunyan, B.; Neukirch, A. J.; Verduzco, R.; Crochet, J. J.; Tretiak, S.; Pedesseau, L.; Even, J.; Alam, M. A.; Gupta, G.; Lou, J.; Ajayan, P. M.; Bedzyk, M. J.; Kanatzidis, M. G.; Mohite, A. D. High-efficiency two-dimensional Ruddlesden-Popper perovskite solar cells. *Nature* **2016**, *536*, 312−316.

(3) Smith, I. C.; Hoke, E. T.; Solis-Ibarra, D.; McGehee, M. D.; Karunadasa, H. I. A layered hybrid perovskite solar-cell absorber with enhanced moisture stability. *Angew. Chem., Int. Ed.* **2014**, *53*, 11232−11235.

(4) Liu, J.; Leng, J.; Wu, K.; Zhang, J.; Jin, S. Observation of Internal Photoinduced Electron and Hole Separation in Hybrid Two-Dimentional Perovskite Films. *J. Am. Chem. Soc.* **2017**, *139*, 1432−1435.

(5) Straus, D. B.; Kagan, C. R. Electrons, Excitons, and Phonons in Two-Dimensional Hybrid Perovskites: Connecting Structural, Optical, and Electronic Properties. *J. Phys. Chem. Lett.* **2018**, *9*, 1434−1447.

(6) Nagasaka, H.; Yoshizawa-Fujita, M.; Takeoka, Y.; Rikukawa, M. Tuning the Structures and Optical Properties of Perovskites by Varying the Alkylamine Type and Chain Length. *ACS Omega* **2018**, *3*, 18925−18929.

(7) Booker, E. P.; Thomas, T. H.; Quarti, C.; Stanton, M. R.; Dashwood, C. D.; Gillett, A. J.; Richter, J. M.; Pearson, A. J.; Davis, N.; Sirringhaus, H.; Price, M. B.; Greenham, N. C.; Beljonne, D.; Dutton, S. E.; Deschler, F. Formation of Long-Lived Color Centers for Broadband Visible Light Emission in Low-Dimensional Layered Perovskites. *J. Am. Chem. Soc.* **2017**, *139*, 18632−18639.

(8) Yin, J.; Li, H.; Cortecchia, D.; Soci, C.; Brédas, J.-L. Excitonic and Polaronic Properties of 2D Hybrid Organic−Inorganic Perovskites. *ACS Energy Lett.* **2017**, *2*, 417−423.

(9) Zhao, C.; Tian, W.; Sun, Q.; Yin, Z.; Leng, J.; Wang, S.; Liu, J.; Wu, K.; Jin, S. Trap-Enabled Long-Distance Carrier Transport in Perovskite Quantum Wells. *J. Am. Chem. Soc.* **2020**, *142*, 15091−15097.

(10) Li, D.; Li, D.; Yang, A.; Zhang, H.; Lai, X.; Liang, C. Electronic and Optical Properties of van der Waals Heterostructures Based on Two-Dimensional Perovskite $(PEA)_2PbI_4$ and Black Phosphorus. *ACS Omega* **2021**, *6*, 20877−20886.

(11) Cao, D. H.; Stoumpos, C. C.; Farha, O. K.; Hupp, J. T.; Kanatzidis, M. G. 2D Homologous Perovskites as Light-Absorbing Materials for Solar Cell Applications. *J. Am. Chem. Soc.* **2015**, *137*, 7843−7850.
(12) Chen, Y.; Sun, Y.; Peng, J.; Tang, J.; Zheng, K.; Liang, Z. 2D Ruddlesden-Popper Perovskites for Optoelectronics. *Adv. Mater.* **2018**, *30*, No. 1703487.
(13) Zhou, J.; Chu, Y.; Huang, J. Photodetectors Based on Two-Dimensional Layer-Structured Hybrid Lead Iodide Perovskite Semiconductors. *ACS Appl. Mater. Interfaces* **2016**, *8*, 25660−25666.
(14) Liao, Y.; Liu, H.; Zhou, W.; Yang, D.; Shang, Y.; Shi, Z.; Li, B.; Jiang, X.; Zhang, L.; Quan, L. N.; Quintero-Bermudez, R.; Sutherland, B. R.; Mi, Q.; Sargent, E. H.; Ning, Z. Highly Oriented Low-Dimensional Tin Halide Perovskites with Enhanced Stability and Photovoltaic Performance. *J. Am. Chem. Soc.* **2017**, *139*, 6693−6699.
(15) Zhang, X.; Munir, R.; Xu, Z.; Liu, Y.; Tsai, H.; Nie, W.; Li, J.; Niu, T.; Smilgies, D. M.; Kanatzidis, M. G.; Mohite, A. D.; Zhao, K.; Amassian, A.; Liu, S. F. Phase Transition Control for High Performance Ruddlesden-Popper Perovskite Solar Cells. *Adv. Mater.* **2018**, *30*, No. 1707166.
(16) He, X.; Wang, Y.; Li, K.; Wang, X.; Liu, P.; Yang, Y.; Liao, Q.; Zhai, T.; Yao, J.; Fu, H. Oriented Growth of Ultrathin Single Crystals of 2D Ruddlesden-Popper Hybrid Lead Iodide Perovskites for High-Performance Photodetectors. *ACS Appl. Mater. Interfaces* **2019**, *11*, 15905−15912.
(17) Yin, T.; Liu, B.; Yan, J.; Fang, Y.; Chen, M.; Chong, W. K.; Jiang, S.; Kuo, J. L.; Fang, J.; Liang, P.; Wei, S.; Loh, K. P.; Sum, T. C.; White, T. J.; Shen, Z. X. Pressure-Engineered Structural and Optical Properties of Two-Dimensional $(C_4H_9NH_3)_2PbI_4$ Perovskite Exfoliated nm-Thin Flakes. *J. Am. Chem. Soc.* **2019**, *141*, 1235−1241.
(18) Fu, R.; Zhao, W.; Wang, L.; Ma, Z.; Xiao, G.; Zou, B. Pressure-Induced Emission toward Harvesting Cold White Light from Warm White Light. *Angew. Chem., Int. Ed.* **2021**, *60*, 10082−10088.
(19) Wang, S.; Ma, J.; Li, W.; Wang, J.; Wang, H.; Shen, H.; Li, J.; Wang, J.; Luo, H.; Li, D. Temperature-Dependent Band Gap in Two-Dimensional Perovskites: Thermal Expansion Interaction and Electron-Phonon Interaction. *J. Phys. Chem. Lett.* **2019**, *10*, 2546−2553.
(20) Guo, S.; Zhao, Y.; Bu, K.; Fu, Y.; Luo, H.; Chen, M.; Hautzinger, M. P.; Wang, Y.; Jin, S.; Yang, W.; Lu, X. Pressure-Suppressed Carrier Trapping Leads to Enhanced Emission in Two-Dimensional Perovskite $(HA)_2(GA)Pb_2I_7$. *Angew. Chem., Int. Ed.* **2020**, *59*, 17533−17539.
(21) Leng, K.; Abdelwahab, I.; Verzhbitskiy, I.; Telychko, M.; Chu, L.; Fu, W.; Chi, X.; Guo, N.; Chen, Z.; Chen, Z.; Zhang, C.; Xu, Q. H.; Lu, J.; Chhowalla, M.; Eda, G.; Loh, K. P. Molecularly thin two-dimensional hybrid perovskites with tunable optoelectronic properties due to reversible surface relaxation. *Nat. Mater.* **2018**, *17*, 908−914.
(22) Wu, X.; Trinh, M. T.; Niesner, D.; Zhu, H.; Norman, Z.; Owen, J. S.; Yaffe, O.; Kudisch, B. J.; Zhu, X. Y. Trap states in lead iodide perovskites. *J. Am. Chem. Soc.* **2015**, *137*, 2089−2096.
(23) De Giorgi, M. L.; Creti, A.; La-Placa, M. G.; Boix, P. P.; Bolink, H. J.; Lomascolo, M.; Anni, M. Amplified spontaneous emission in thin films of quasi-2D $BA_3MA_3Pb_5Br_{16}$ lead halide perovskites. *Nanoscale* **2021**, *13*, 8893−8900.
(24) Ghosh, S.; Pradhan, B.; Zhang, Y.; Hofkens, J.; Karki, K. J.; Materny, A. Nature of the different emissive states and strong exciton-phonon couplings in quasi-two-dimensional perovskites derived from phase-modulated two-photon micro-photoluminescence spectroscopy. *Phys. Chem. Chem. Phys.* **2021**, *23*, 3983−3992.
(25) Billing, D. G.; Lemmerer, A. Synthesis, characterization and phase transitions of the inorganic−organic layered perovskite-type hybrids $[(C_nH_{2n+1}NH_3)_2PbI_4]$ (n = 12, 14, 16 and 18). *New J. Chem.* **2008**, *32*, 1736−1746.
(26) Lemmerer, A.; Billing, D. G. Synthesis, characterization and phase transitions of the inorganic-organic layered perovskite-type hybrids $[(C_nH_{2n+1}NH_3)_2PbI_4]$, n = 7, 8, 9 and 10. *Dalton Trans.* **2012**, *41*, 1146−1157.
(27) Billing, D. G.; Lemmerer, A. Synthesis, characterization and phase transitions in the inorganic-organic layered perovskite-type hybrids $[(C_nH_{2n+1}NH_3)_2PbI_4]$, n = 4, 5 and 6. *Acta Crystallogr., Sect. B: Struct. Sci.* **2007**, *63*, 735−747.
(28) Amerling, E.; Baniya, S.; Lafalce, E.; Zhang, C.; Vardeny, Z. V.; Whittaker-Brooks, L. Electroabsorption Spectroscopy Studies of $(C_4H_9NH_3)_2PbI_4$ Organic-Inorganic Hybrid Perovskite Multiple Quantum Wells. *J. Phys. Chem. Lett.* **2017**, *8*, 4557−4564.
(29) Sheikh, T.; Shinde, A.; Mahamuni, S.; Nag, A. Possible Dual Bandgap in $(C_4H_9NH_3)_2PbI_4$ 2D Layered Perovskite: Single-Crystal and Exfoliated Few-Layer. *ACS Energy Lett.* **2018**, *3*, 2940−2946.
(30) Dobrovolsky, A.; Merdasa, A.; Unger, E. L.; Yartsev, A.; Scheblykin, I. G. Defect-induced local variation of crystal phase transition temperature in metal-halide perovskites. *Nat. Commun.* **2017**, *8*, No. 34.
(31) Ma, J.-P.; Yin, J.; Chen, Y.-M.; Zhao, Q.; Zhou, Y.; Li, H.; Kuroiwa, Y.; Moriyoshi, C.; Li, Z.-Y.; Bakr, O. M.; Mohammed, O. F.; Sun, H.-T. Defect-Triggered Phase Transition in Cesium Lead Halide Perovskite Nanocrystals. *ACS Mater. Lett.* **2019**, *1*, 185−191.
(32) Stoumpos, C. C.; Cao, D. H.; Clark, D. J.; Young, J.; Rondinelli, J. M.; Jang, J. I.; Hupp, J. T.; Kanatzidis, M. G. Ruddlesden-Popper Hybrid Lead Iodide Perovskite 2D Homologous Semiconductors. *Chem. Mater.* **2016**, *28*, 2852−2867.
(33) Mondal, N.; Naphade, R.; Zhou, X.; Zheng, Y.; Lee, K.; Gereige, I.; Al-Saggaf, A.; Bakr, O. M.; Mohammed, O. F.; Gartstein, Y. N.; Malko, A. V. Dynamical Interconversion between Excitons and Geminate Charge Pairs in Two-Dimensional Perovskite Layers Described by the Onsager-Braun Model. *J. Phys. Chem. Lett.* **2020**, *11*, 1112−1119.
(34) Smith, M. D.; Karunadasa, H. I. White-Light Emission from Layered Halide Perovskites. *Acc. Chem. Res.* **2018**, *51*, 619−627.
(35) Hu, T.; Smith, M. D.; Dohner, E. R.; Sher, M.-J.; Wu, X.; Trinh, M. T.; Fisher, A.; Corbett, J.; Zhu, X. Y.; Karunadasa, H. I.; Lindenberg, A. M. Mechanism for Broadband White-Light Emission from Two-Dimensional (110) Hybrid Perovskites. *J. Phys. Chem. Lett.* **2016**, *7*, 2258−2263.
(36) Krishnamurthy, S.; Naphade, R.; Mir, W. J.; Gosavi, S.; Chakraborty, S.; Vaidhyanathan, R.; Ogale, S. Molecular and Self-Trapped Excitonic Contributions to the Broadband Luminescence in Diamine-Based Low-Dimensional Hybrid Perovskite Systems. *Adv. Opt. Mater.* **2018**, *6*, No. 1800751.
(37) Abdi-Jalebi, M.; Andaji-Garmaroudi, Z.; Cacovich, S.; Stavrakas, C.; Philippe, B.; Richter, J. M.; Alsari, M.; Booker, E. P.; Hutter, E. M.; Pearson, A. J.; Lilliu, S.; Savenije, T. J.; Rensmo, H.; Divitini, G.; Ducati, C.; Friend, R. H.; Stranks, S. D. Maximizing and stabilizing luminescence from halide perovskites with potassium passivation. *Nature* **2018**, *555*, 497−501.
(38) Stewart, R. J.; Grieco, C.; Larsen, A. V.; Doucette, G. S.; Asbury, J. B. Molecular Origins of Defects in Organohalide Perovskites and Their Influence on Charge Carrier Dynamics. *J. Phys. Chem. C* **2016**, *120*, 12392−12402.
(39) Zheng, X.; Chen, B.; Dai, J.; Fang, Y.; Bai, Y.; Lin, Y.; Wei, H.; Zeng, X. C.; Xiao, C.; Huang, J. Defect passivation in hybrid perovskite solar cells using quaternary ammonium halide anions and cations. *Nat. Energy* **2017**, *2*, No. 17102.
(40) Chu, W.; Zheng, Q.; Prezhdo, O. V.; Zhao, J.; Saidi, W. A. Low-frequency lattice phonons in halide perovskites explain high defect tolerance toward electron-hole recombination. *Sci. Adv.* **2020**, *6*, No. aaw7453.

https://doi.org/10.1021/acsomega.1c04800
ACS Omega 2021, 6, 35427−35432